Long-wavelength lithospheric magnetic field of China

Yi Jiang[1,2,4,6*], Richard Holme[2], Sheng-Qing Xiong[3*], Yong Jiang[1,5], Yan Feng[1,4,6], Hai Yang[3]

1. Institute of Space Weather, Nanjing University of Information Science and Technology, Nanjing 210044, China
2. School of Environmental Sciences, University of Liverpool, L69 3GP, UK
3. China Aero Geophysical Survey and Remote Sensing Center for Natural Resource, Beijing 100083, China
4. State Key Laboratory of Lunar and Planetary Sciences, Macau University of Science and Technology, Taipa 999078, Macau, China
5. Scotland Academy at WXU, Wuxi Taihu University, Wuxi 214064, China
6. State Key Laboratory of Space Weather, Chinese Academy of Sciences, Beijing 100190, China

Summary

We present new regional models, denoted CLAS, of the Chinese lithospheric field, combining the long wavelength information provided by satellite-derived models: CHAOS-6, MF7, LCS-1 and NGDC720, and an extremely high-quality compilation of 97994 aeromagnetic survey data with 10km×10km resolution for shorter wavelength. The models are estimated using a depleted basis of global spherical harmonic functions centred on China. CLAS models are determined include harmonic degrees up to 400. Although some accuracy of aeromagnetic data is lost in order to balance the consistent of two data sets, the results show that CLAS models have a high correlation with the satellite models at low degree terms (degree correlation>0.9) but with more power at high degree terms, reflecting more features of the lithospheric field in continental China. Examples of improvement include Changbai mountains, Sichuan Basin and Qinghai-Tibet Plateau. CLAS models have good agreement (coherence>0.9) with Chinese aeromagnetic data at wavelength down to about 100km (corresponding to spherical harmonic degree n=400), filling the usual gap between satellite models and aeromagnetic data. Comparison with aeromagnetic data filtered at 100 km gives good agreement (correlation>0.95). The residuals between CLAS models and aeromagnetic data are still large (RMS>70nT), but with most of misfits arising from shorter wavelength fields that the model cannot fit at degree up to 400; such misfit could be reduced by increasing the model degree. We provide a geological example of how the inclusion of satellite data can change the geological conclusions that can be drawn from the magnetic information. However, the two data sets are not completely consistent, future models should start from a reanalysis of the aeromagnetic data and its line leveling to ensure consistency with the satellite model.

Key words: Composition and structure of the continental crust, Inverse theory,

Magnetic anomalies: modelling and interpretation, Satellite magnetics, Spatial analysis.

Introduction

The internal geomagnetic field is dominated by sources in the deep Earth (the core field) and the near surface (the "crustal field", or more accurately the field from the lithosphere). Interpretation of the global geomagnetic spectrum suggests the core field dominates spherical harmonic degrees 1 to ~14 (wavelengths at the surface greater than 3000km) with surface sources dominant at higher degree / shorter wavelength.

Derivation of a magnetic field model can utilizes various magnetic data sources, which can be obtained by ground, marine, aerial, balloon, or satellite. Aeromagnetic data particularly reflect short wavelength components of the lithospheric field. Thus, the field of the upper crust (above degree 150) can be modelled by aeromagnetic data (Hemant et al., 2007). However, due to the limited and uneven distribution of ground observations, magnetic anomalies with large wavelengths of more than 500 km are not always reliably determined (Thébault et al., 2010). The long wavelength components of the lithospheric field cannot be completely retained, losing resolution between perhaps 200km wavelength up to 3000km (above which the core field becomes dominant).

In contrast, satellite data constrain the field at lower harmonic degrees, even though the wavelengths will be attenuated at satellite altitude. During the past five decades, satellite data collected from POGO, MAGSAT, CHAMP, Ørsted, SAC-C and Swarm have played an important role in the study of the lithospheric field, since it is of high-quality and a global perspective. The most widely used models, such as the CHAOS model series (Olsen et al., 2014; Finlay et al., 2015; 2016), the MF model series (Maus et al., 2007; 2008; Maus, 2010a) and the comprehensive model (CM) series (Sabaka et al., 2004, 2015) are derived by satellite data from the satellites CHAMP, Ørsted, SAC-C and Swarm. These models contain all the coherent structure that the satellite data possess, and provide a very good constraint on the long wavelength lithospheric field. However, there is still in general a gap between satellite models and aeromagnetic data.

There has been considerable recent progress on the resolution to shorter wavelengths of the field due to data from the Swarm satellites and its modelling, such that there is now overlap with crustal moedlling for some areas [for example Australia flew a number of coast to coast aeromagnetic flights to collect the long wavelength contributions (Milligan et al., 2010)] between the satellite and aeromagnetic data. A recent major advance in satellite modelling is the LCS-1 model of Olsen et al. (2017) which provides accuracy up to spherical harmonic degree 185 (wavelengths of longer than 216km), and shows strong coherence with studies from the aeromagnetic data. Ou et al. (2013) and Feng et al. (2016a; 2016b; 2018) also studied the lithospheric magnetic field in China through satellite and ground-based data. Nevertheless, comparing with aeromagnetic compilation of continental China (Xiong et al., 2016a), though the map of the lithospheric field extracted from this model has some clearly

common features, there are also clear offsets between regions.

The quality of the aeromagnetic compilation of Xiong et al. (2016b) is extremely high, but a detailed comparison with satellite models over China have not been made, compared with for example Australia and North America (Ravat & Korhonen, 2009). Thus, the two data sets are truly independent. It therefore seems highly likely that the best model of the field for China could be constructed by combining the satellite models and aeromagnetic data, giving a model with all wavelengths below 3000km. A global representation of the lithospheric field is provided by the World Digital Magnetic anomaly map (WDMAM) (Lesur et al., 2016). It is hoped that our work will contribute to this project, but currently this project lacks high-resolution Chinese data, and so direct comparison of the two models is misleading.

Other methods have been applied to combine the constraint of both satellite and ground-based data. For example, spherical cap harmonics (Haines, 1985; Thébault et al., 2006), are popular in the literature, but have poor convergence properties at the boundaries and are not well-suited to model data of varying heights, making the combination of satellite and ground data difficult. Slepian functions (Simons et al., 2006; Baggan et al., 2013) are more powerful, but further from conventional modeling understanding. We have attempted modeling simultaneously with satellite and ground-based data, but have found this approach not to be optimal – in particular, the difference in treatment necessary for ionospheric and magnetospheric data considerably increases the complexity of the problem. Such simultaneous fitting has been applied through the Comprehensive modeling programme (Sabaka et al., 2004; 2015) but that approach is fully global, and does not allow focus on the more detailed regional constraints that we consider here. This method is not computationally possible to resolve smaller scale field structure. Our approach applies global models as the best way to consider constraint from satellite data, by allowing the information from these models not to be fixed (particularly at wavelengths at the limit of the resolution of satellite data, where the field structure is only marginally constrained by satellite observations), but to be varied to best allow simultaneous fit to the aeromagnetic data.

Therefore, to better combine the information of Chinese aeromagnetic data with the constraint of measurements from satellite surveys, we present a new regional model of the lithospheric magnetic field, based on a depleted basis of global spherical harmonic functions. We denote our new models CLAS (Chinese Lithospheric model derived from Aeromagnetic data and Satellite models), with a number stating the truncation degree of the model, such as CLAS185 and CLAS400. Section 2 and Section 3 describe the data and method respectively. The result and discussion of new Chinese Lithospheric field models are presented in Section 4. Section 5 summaries our work, and considers broader implications for geomagnetic field modelling.

Data

Our magnetic “data” are at ground level a compilation of the Chinese aeromagnetic

survey, and for the Swarm satellite mission a derived global geomagnetic model. The aeromagnetic map is that of Xiong et al (2016), based on aeromagnetic survey from China Aero Geophysical Survey and Remote Sensing Center for Natural Resource between 1970 and 2011. The resolution of the map is 10 km×10 km, including 97994 valid values that cover 979.6 km^2. Figure 1 is a map of the aeromagnetic scalar data for continental China.

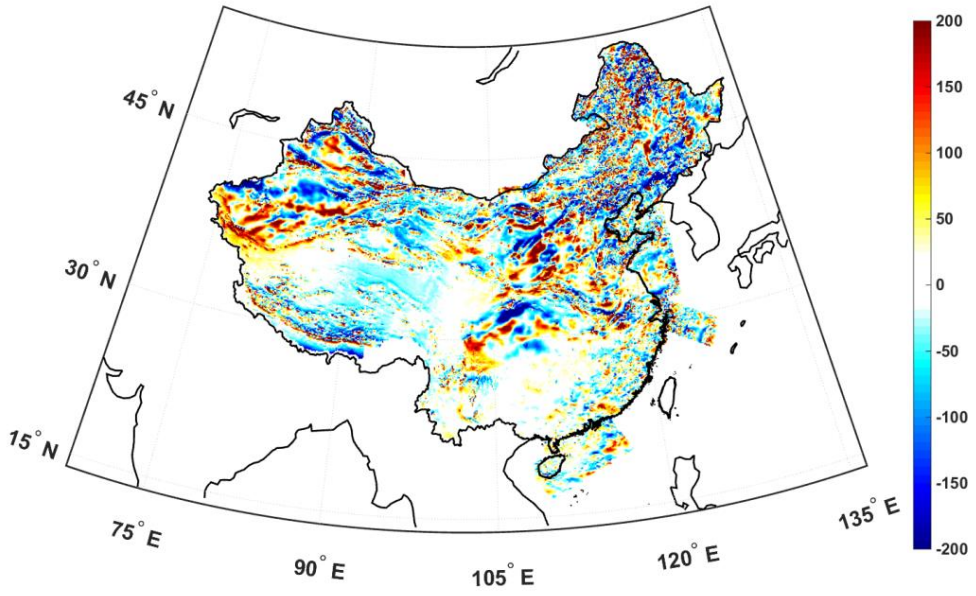

Fig 1. The aeromagnetic map of continental China at 1km（ΔF）

Swarm satellite mission (Friis-Christensen et al., 2006) comprises three dedicated low-Earth-orbit satellites that launched in November 2013. Two of them (Swarm-A and Swarm-C) fly side by side at orbits of inclination 87.4°, about 440 and 450 km altitude respectively (as of 2019 August). Another one (Swarm-B) is in a higher 520 km orbit (as of 2019 August) with an inclination of 88°.

The Swarm data have great potential to increase understanding of the lithospheric field. However, direct modeling of the data is complicated by time-variable sources of external field, and the varying information content of vector differences in measurements due to changing satellite positions. It is most straightforward to constrain the lithospheric field using a field model rather than directly with the satellite data from which it is derived. The models contain all the coherent structure that the satellite data possess. We selected satellite magnetic field models, CHAOS-6, MF7, LCS-1 and NGDC720, instead of satellite data, and combine aeromagnetic map to study the lithospheric field in China. These models, developed by Finlay et al. (2016), Maus et al. (2010a; 2010b), Olsen et al. (2017), describe the internal magnetic field up to degree n=120, 133, 185 and 720, respectively.

Method

A depleted basis of global spherical harmonic functions is used to model lithospheric field in China. Since the lithosphere magnetic field is independent of time, the internal field

can be represented as the gradient of a scalar potential $(\mathbf{B} = -\nabla\mathbf{V})$, with the potential satisfying Laplace's equation, expanded in spherical harmonics

$$V = a\sum_{n=1}^{N}\sum_{m=0}^{n}\left[g_n^m \cos m\lambda + h_n^m \sin m\lambda \right]\times\left(\frac{a}{r}\right)^{n+1} P_n^m\left(\cos\theta\right) \qquad (1)$$

where a=6371.2km is the radius of the Earth, (θ,λ,r) are the geographical coordinate system (colatitude, longitude, spherical radial distance), $\left\{g_n^m, h_n^m\right\}$ are the Gauss coefficients and $P_n^m\left(\cos\theta\right)$ are the Schmidt semi-normalized associated Legendre functions of degree n and order m.

While we use global functions, clearly the data distribution is restricted to the local area (in this case China), and therefore there is no constraint on the structure of the field elsewhere. As a result, linear combinations of the spherical harmonic components that are of low amplitude in China remain unconstrained and the model nonunique. We seek only values for the model parameters that are constrained by the data, with other components damped or eliminated to reduce or eliminate unconstrained structure. China is conveniently shaped that we consider a spherical cap which covers the data area. We derive eigenvectors of the Gauss coefficients to model the data assuming a cap centred on the north pole with assumed uniform data distribution, such that eigenvectors of harmonics of different spherical harmonic order are orthogonal. Eigenvectors with very small eigenvalues (which are not constrained by information near the pole) are assumed to have a value of zero. We then rotate the coordinate system so that it is centred on China, and solve for coefficients of the reduced basis. A similar effect is achieved by using a local basis, for example spherical cap harmonics, but we choose to use global spherical harmonics to provide a better stability and understanding of upward and downward continuation, to allow for easier unification of constraint from ground and satellite measurements.

To model continental China we consider the range is 18°*N*-54°*N*, 73°*E*-136°*E*, we describe magnetic field $\mathbf{B} = \mathbf{Am}$, where $\mathbf{A}$ is a spherical harmonic of a polar cap (centered on the North pole, colatitude 0-30 degree, and all longitudes) and enough to cover continental China. We consider a uniform data $\mathbf{B}$ distribution around this polar cap of vector field measurements, and $\mathbf{m} = \left\{g_n^m, h_n^m\right\}$ is a vector of the Gauss coefficients. Using these data locations, we obtain a normal equations matrix $\mathbf{A^T A}$, and from this eigenvalues λ and eigenvectors $\mathbf{V} = \left\{q_n^m, s_n^m\right\}$ of linear combinations of spherical harmonics which provide the natural basis of the solution.

Using such a basis provides two reductions in complexity of the system. The first is that we eliminate a large proportion of the eigenvectors as there will be many combinations of spherical harmonics with small eigenvalues that have no significant amplitude of the vector field components within the cap. Only the eigenvectors that have large eigenvalue were

considered in the solution, by applying a form of ranking and winnowing. In deriving the new regional lithospheric field model, when truncating at degree 120, 133, 185 and 400, we use 1454, 1468, 3371 and 9436 eigenvectors from a total possible number of 14640, 17955, 34595 and 160800, respectively, saving more than 90% of the calculation.

The second simplification comes from symmetry as our basis functions are calculated assuming that the data distribution is symmetric and uniform about the poles. This is not the case, but we assume that the data distribution is sufficiently dense that such an approximation is useful. The spherical harmonic system separates in order m of the spherical harmonics, so that the normal equations matrix becomes block diagonal. The matrix can be divided by a large set of small matrices of order $2N$ or less, instead of having to solve for a full matrix of dimension $N(N+2)$, where N is the maximum degree truncation. This provides a substantial saving in the evaluation time of the solution process.

To obtain the solution in the area of continental China, we construct a new coordinate system (Θ, Λ) with the pole at the center of continental China (36°*N*, 104.5°*E*). Rotating the basis functions into the new coordinate system following De Santis et al. (1996), their eqs (2), as follows

$$P_n^m(\cos\theta)\begin{Bmatrix}\cos m\lambda\\ \sin m\lambda\end{Bmatrix} = \sum_{\mu=0}^{n}\left[\begin{Bmatrix}a_{n,\mu}^m\\ c_{n,\mu}^m\end{Bmatrix}\cos\mu\Lambda + \begin{Bmatrix}b_{n,\mu}^m\\ d_{n,\mu}^m\end{Bmatrix}\sin\mu\Lambda + \right] P_n^m(\cos\Theta) \tag{2}$$

where $a_{n,\mu}^m, b_{n,\mu}^m, c_{n,\mu}^m, d_{n,\mu}^m$ are parameters for the rotation, and the set of functions in the new coordinate system $\tilde{\mathbf{V}} = \{\tilde{q}_n^m, \tilde{s}_n^m\}$ in terms of the set $\mathbf{V} = \{q_n^m, s_n^m\}$:

$$\begin{aligned}\tilde{q}_n^m &= \sum_{\mu=0}^{n}\left[a_{n,m}^{\mu} q_n^{\mu} + c_{n,m}^{\mu} s_n^{\mu}\right]\\ \tilde{s}_n^m &= \sum_{\mu=0}^{n}\left[b_{n,m}^{\mu} q_n^{\mu} + d_{n,m}^{\mu} s_n^{\mu}\right]\end{aligned} \tag{3}$$

Scalar data (i.e. magnetic field total intensity) from aeromagnetic data can be treated by these eigenvectors as follow

$$\mathbf{E} = \mathbf{B}_{\text{aero}} - \mathbf{B}_{\text{mod}} \tag{4}$$

$$\mathbf{E} = \tilde{\mathbf{A}}\tilde{\mathbf{V}}\mathbf{e} \tag{5}$$

where $\mathbf{E}$ are residuals between aeromagnetic data $\mathbf{B}_{\text{aero}}$ and satellite models $\mathbf{B}_{\text{mod}}$, $\tilde{\mathbf{A}}$ are data kernels matrix in China, and $\mathbf{e}$ is a set of coefficients of the Gauss coefficients given by eigenvectors, which can be estimated using least-squares algorithm as follows

$$\mathbf{e} = \left(\left(\tilde{\mathbf{A}}\tilde{\mathbf{V}}\right)^{\mathrm{T}}\tilde{\mathbf{A}}\tilde{\mathbf{V}}\right)^{-1}\left(\tilde{\mathbf{A}}\tilde{\mathbf{V}}\right)^{\mathrm{T}}\mathbf{E} \tag{6}$$

The final result in terms of the Gauss coefficients $\tilde{\mathbf{m}} = \{\tilde{g}_n^m, \tilde{h}_n^m\}$ can be represented by recombining all the eigenvectors scaled by these coefficients, and added to the coefficients of the initial model $\mathbf{m}$:

$$\tilde{\mathbf{m}} = \tilde{\mathbf{V}}\mathbf{e} + \mathbf{m} \tag{7}$$

The coefficients of CHAOS-6, MF7, LCS-1 and NGDC720 model are provided as initial coefficients, the maximum of almost 10000 parameters were estimated from 97994 aeromagnetic observations in deriving four new regional models at degree 120, 133, 185 and 400, respectively.

In addition to fitting the aeromagnetic data, a side constraint is imposed to unify this calculation with the satellite model. We minimise $(n+1)\left(\tilde{g}_n^m - g_n^m\right)^2$, the difference in mean square field, defined at satellite altitude, and applied as a damping term to the matrix before solution of the eigenvectors. For ease of calculation, the normalization of the parameters is changed so that the damping matrix is the identity matrix; then the eigenvectors are independent of damping and the range of damping can be explored for only one eigensystem calculation. A large damping term biases the model strongly to the corresponding prior satellite model which will make the model lose the characteristics of aeromagnetic data. In contrast, a small damping term will lead to a model closer fitting the aeromagnetic data; however, it will have a boundary effects at satellite altitude. Therefore, the end result of an appropriate intermediate damping choice is that the large scale low degree terms will be constrained by the satellite model, whereas the small scale, high degree terms will be constrained by the Chinese aeromagnetic data.

Results and discussion

Damping

Based on CHAOS-6, MF7 and LCS-1 model, we fit the aeromagnetic data and derived new regional models with equivalent spherical harmonic degree to the constraining model. For a higher degree model, a new regional model of degree 400 combines NGDC720 and Chinese aeromagnetic grid. However, the compilation of the aeromagnetic data requires detrending of aeromagnetic flight data, which leads to inconsistencies with the satellite models. Applying the damping more heavily means a closer fit to the satellite model, but will down weight the ground data. In contrast, weaker damping will let the model close to the aeromagnetic data, but it will be bad for upward continuation, and “ringing” at the boundary is worse at satellite altitude. Therefore, a balance needs to be found between two data sets. Fig. 2 shows the root-mean-squared (RMS) trends between CLAS models and different data sets under different damping. RMS is calculated by evaluating the F of the CLAS model for the ground data. When the damping is strong (here 10^{10}), the CLAS models are close to their corresponding a priori models. For aeromagnetic data, the RMS increases with increased damping. There is distinct jump when the damping is raised to 10^7. For the Swarm a priori model, the models at damping 10^2 are far from that model; however, with increased damping, their RMS drops rapidly and eventually stabilizes.

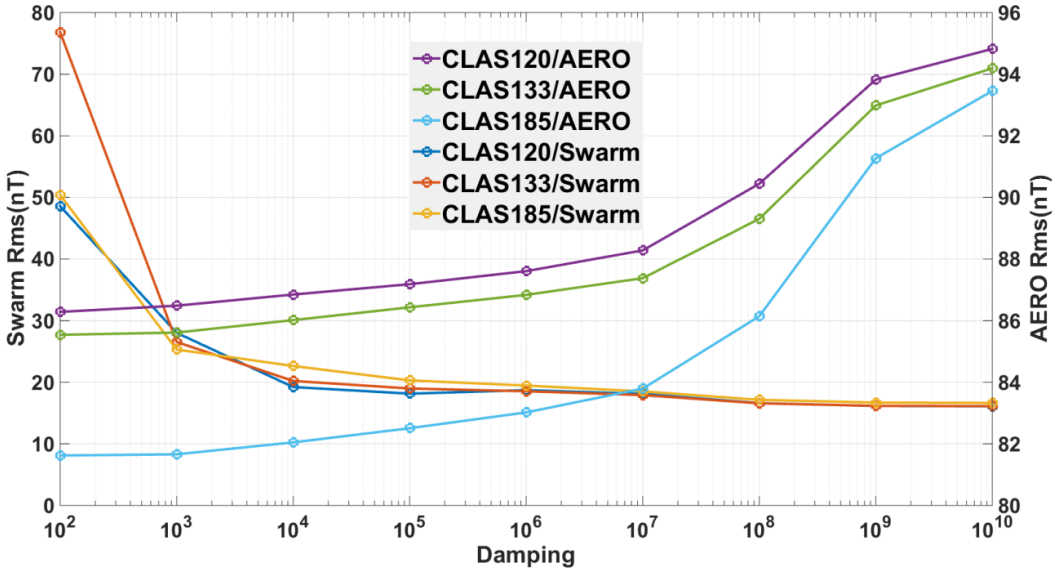

Fig 2. RMS between CLAS models and data under different damping. Units are nT.

Left: RMS from CLAS models and Swarm satellite data.

Right: RMS from CLAS models and Aeromagnetic data.

In addition, a small damping will lead the CLAS models more closely fitting the aeromagnetic data, thus having a better plot on the ground. However, at the same time, it will have a boundary effects at satellite altitude. This effect will become more obvious as the height increases. To optimize the trade-off between fits to ground and satellite constrains, the damping is chosen to be 10^7. Large variations at boundaries effects are mitigated by controlling the fit to the satellite models; aeromagnetic features can still be resolved on the ground.

Spatial distribution

Scalar anomaly maps of CLAS models at Earth surface over continental China are represented in Fig. 3, with the truncation at degree 120,133, 185 and 400. For comparison, Fig. 3 also shows the maps of CHAOS-6, MF7, LCS-1 and NGDC720 model (this last truncated at degree 400).

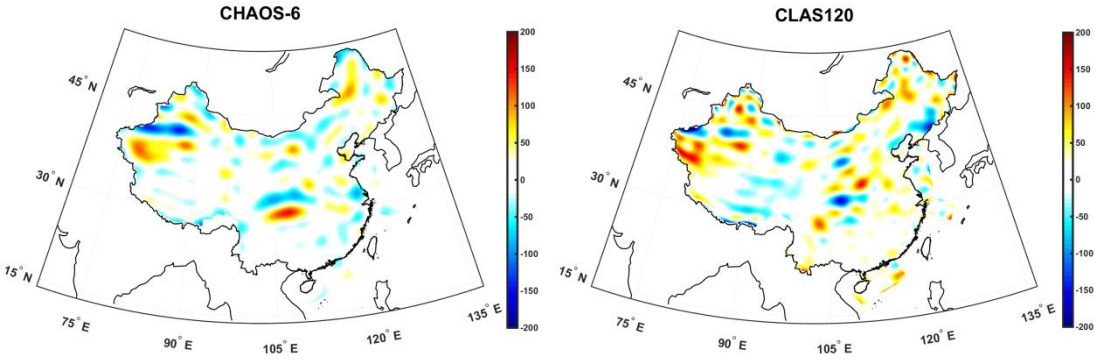

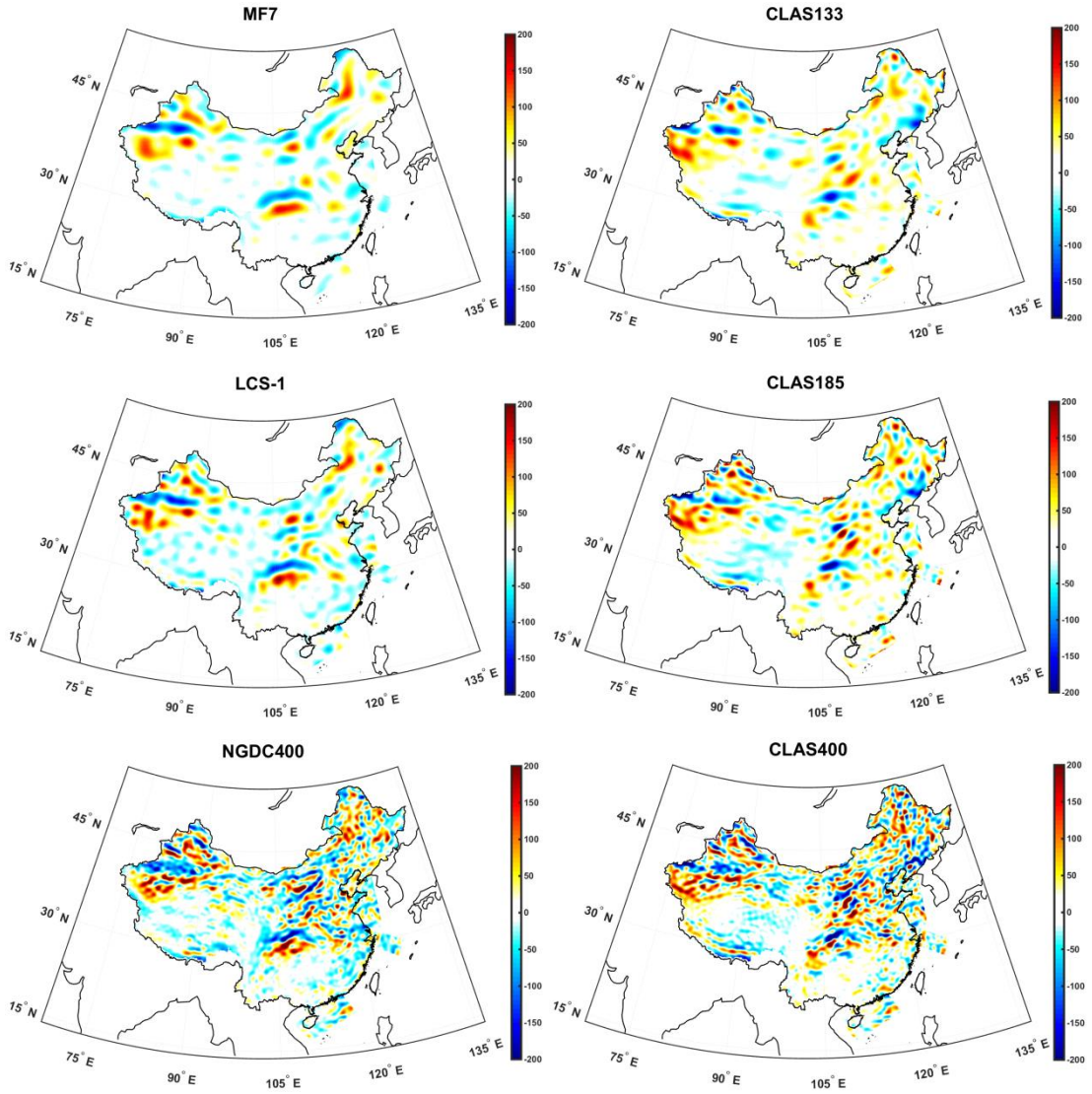

Fig 3. Lithospheric magnetic field Maps of scalar anomaly *F* in continental China at a reference Earth surface datum. Units are nT.

Top panel: from CHAOS-6 (left) and CLAS120 (right) for SH degrees up to 120.

Second panel: from MF7 (left) and CLAS133 (right) for SH degrees up to 133.

Third panel: from LCS-1 (left) and CLAS185 (right) for SH degrees up to 185.

Bottom panel: from NGDC (left) and CLAS400 (right) for SH degrees up to 400.

For all models in Fig.3, the strongest long wavelength magnetic anomalies in continental China are concentrated to the northwest, northeast and central regions of China. For new regional models CLAS, the overall distribution of Chinese lithospheric field is similar: in the northeastern part of China, some positive magnetic anomalies can be found in eastern Inner Mongolia with a maximum intensity of 291nT, while negative magnetic anomalies are concentrated in the Changbai Mountains and the total intensity reaches -157.5nT. For northwest China, a large area of magnetic anomalies is shown in Xinjiang, positive anomalies (up to 291nT) in Tarim Basin and Junggar Basin, and negative anomalies (about -308nT) at Tianshan Mountains. South of this area, Qinghai-Tibet Plateau has a wide range of magnetic

anomalies but with low negative intensity, and its intensity is enhanced compared with the satellite models near the Himalayas. In addition, central China shows substantial positive and negative magnetic anomalies, especially large-scale anomalies in the Sichuan Basin. CLAS400 provides more small-scale structures, particularly in northern China than other CLAS models due to its higher resolution.

Compared with satellite models, the maps of the lithospheric field extracted from these models have some clear common features, but there are also clear offsets between regions. CLAS models have higher horizontal resolution, which shows more features on the map that satellite models do not demonstrate, for example, negative magnetic anomalies in Changbai Mountains and Qinghai-Tibet Plateau. Besides, the new model also differs from satellite models in certain lithosphere magnetic field features, especially in central China. In this area, there are two distinct areas of positive and negative magnetic anomalies. The negative magnetic anomaly area has shrunk, and the positive magnetic anomalies are on the west side of the place which satellite models displayed. CLAS gives more details splitting large scale structure shown by satellite models.

To examine the complementary fit at satellite altitude, Fig.4 plots LCS-1, NGDC, CLAS185 and CLAS400 at 500km.

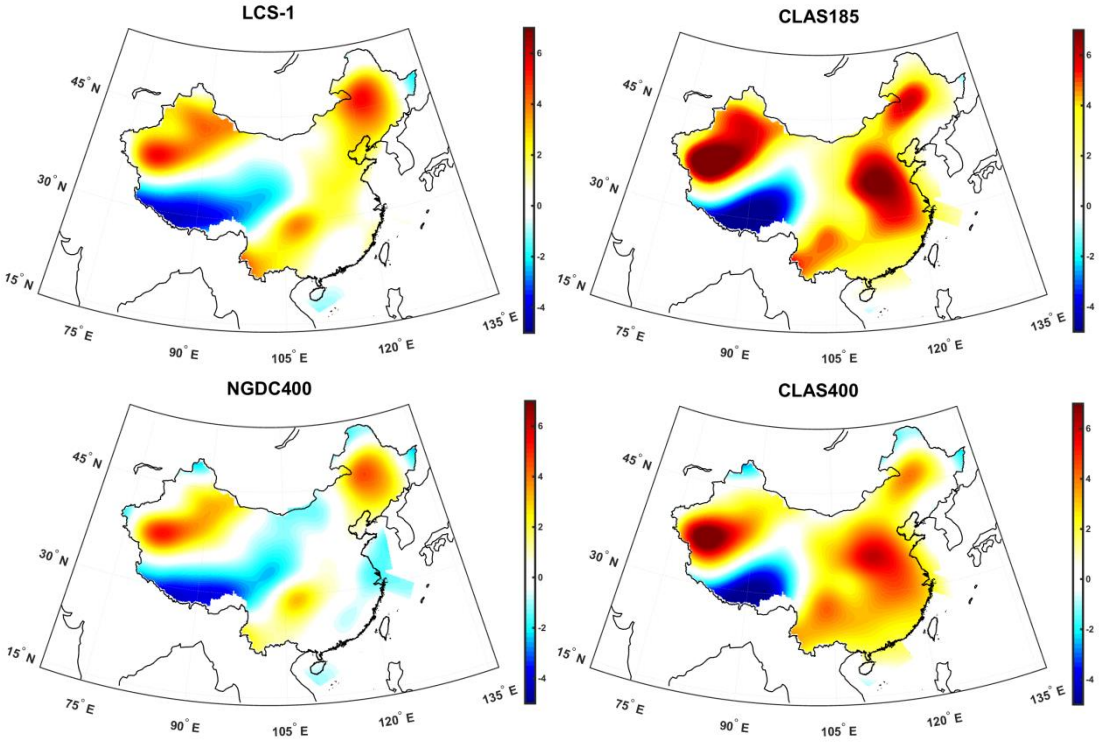

Fig 4. Lithospheric magnetic field Maps of scalar anomaly *F* in continental China at 500km altitude. Units are nT.

Top panel: from LCS-1 (left) and CLAS185 (right) for SH degrees up to 185.

Bottom panel: from NGDC (left) and CLAS400 (right) for SH degrees up to 400.

The pattern shows good agreement at 500km. The positive magnetic anomaly in Xinjiang, northwest of China and the negative magnetic anomaly in Qinghai-Tibet Plateau, can be seen

in all maps in Fig 4. Positive anomalies are also seen over northeast of China too; they are not identical, but this is because the aeromagnetic data impose some long wavelength structure which deviates from the satellite model. For instance, compared with LCS-1 and NGDC, the positive anomaly features of northeast and southwest are weakened in the CLAS models. CLAS models also show a positive anomaly in East China, not seen in satellite models. These differences suggest that the treatment of long wavelength components of the crustal model is not adequate.

Residual

To evaluate the CLAS models, model residuals to the Chinese aeromagnetic data $\mathbf{E} = \mathbf{B}_{data} - \mathbf{B}_{\mathrm{mod}}$ are shown in Fig. 5 and Fig. 6.

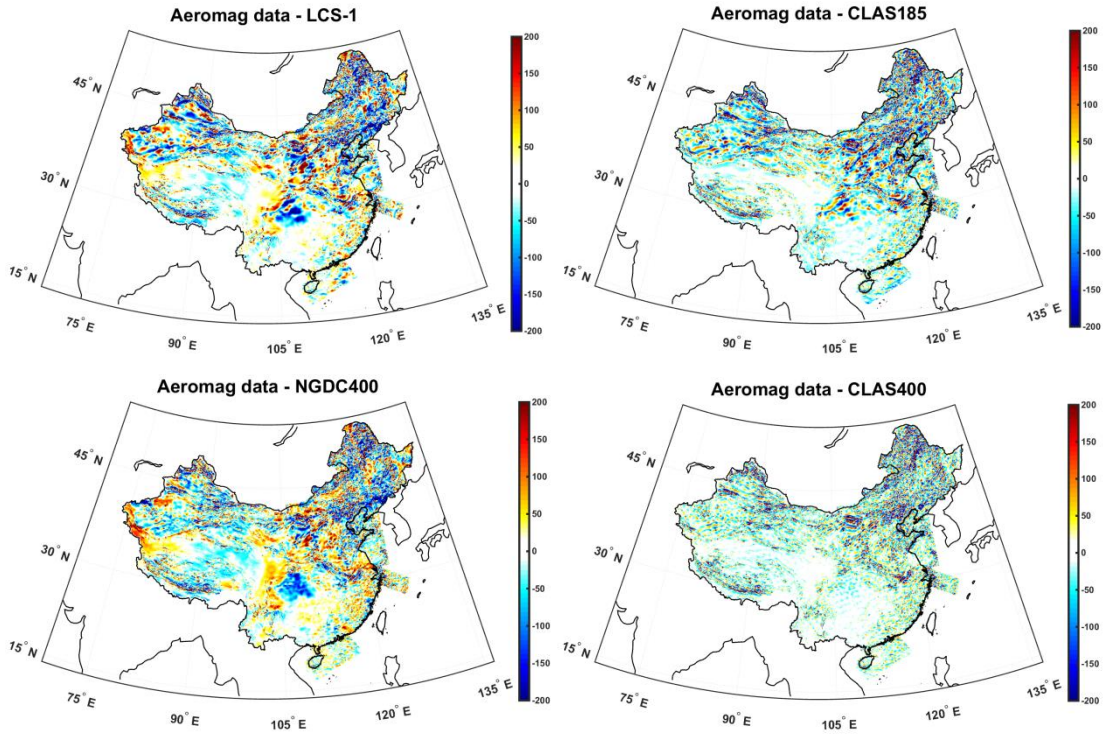

Fig 5. Spatial comparison of the residuals (scalar anomaly *F*) between aeromagnetic data and models. Units are nT.

Top: from Data-LCS-1 (left) and Data-CLSA185 (right).

Bottom: from Data-NGDC400 (left) and Data-CLSA400 (right).

The differences in the residual plots demonstrate that the new models are reflecting the data, and not being restricted by the input models. However significant differences can be seen in the Fig.5. A substantial misfit still exists between model and data, particularly in north and southwest of China. Much of this is small-scale with wavelength less than 200km, below the resolution of the models at SH degree 185. Even CLAS400 display the same problem. On the other hand, although the RMS values of models are similar (CHAOS-6 to CLAS120 94.96nT to 88.28nT, MF7 to CLAS133 94.36nT to 87.38nT, LCS-1 to CLAS185 93.8nT to 83.79nT and NGDC400 to CLAS400 86.27nT to 71.17nT), the residual maps presented by the

CLAS400 show that new models narrow the gap with aeromagnetic data: residuals in West and Central China have clearly decreased.

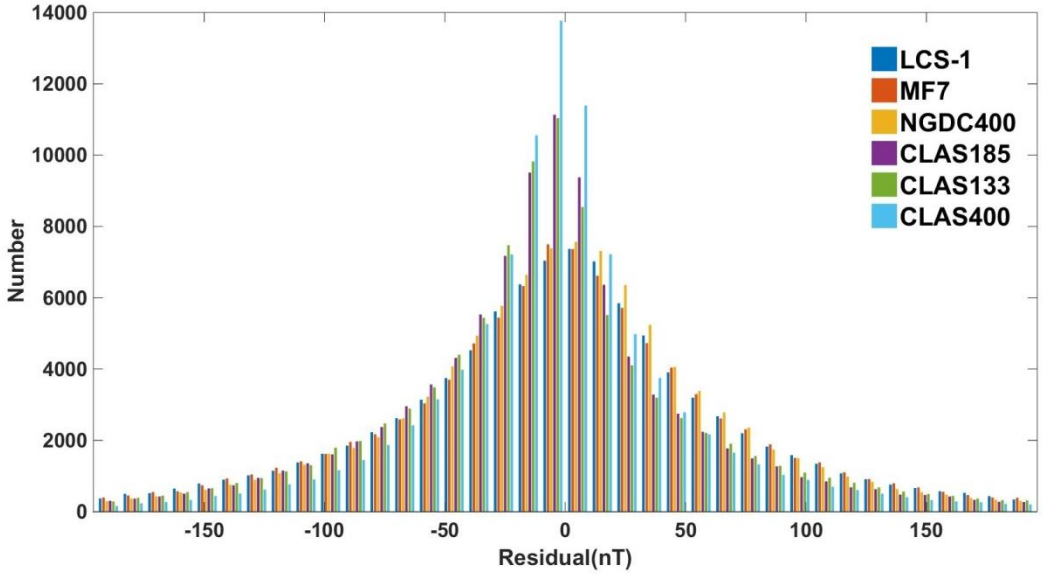

Fig 6. Statistical distribution of model residuals (outliers discarded).

Fig. 6 illustrate the statistical distribution of residuals for various models. The distributions for CLAS models have obvious improvements over the satellite models. The scatter of residuals is smallest for CLAS400 model (light blue bars). For the number of points that model residuals with less than ±10nT, CLAS models have 24619, 20010 and 19158, corresponding to CLAS400, CLAS185 (purple bars) and CLAS133 (green bars), respectively. But only 14588 for NGDC model (yellow bars), 14078 for LCS-1 (deep blue bars) and 14501 for MF7 (orange bars). On the other hand, in the part where the residuals are greater than ± 200nT, the percentage of the satellite models and the CLAS models in 97994 aeromagnetic data are nearly 4.52% and 3.12%, respectively. The model residuals are still large because of the small-scale structure of the lithosphere magnetic field that cannot be fit at 400 degrees. As models are enhanced from increased truncation degree, the residuals and RMS are reduced. In the comparison with 28662 Swarm data in China region, the accuracy of the CLAS model is as expected slightly lower than that of the corresponding satellite models.

Although the lithospheric field model is limited to long wavelength, and so can not fit the small-scale structure, a comparison of the model and data can be made easier by eliminating short wavelength features using along-track averaging of the data over latitude or longitude. We analyse the transect and running average (Fig. 7) of the models and data grid to test whether there is a large spatial jump in the data because of incorrect background matching in the model.

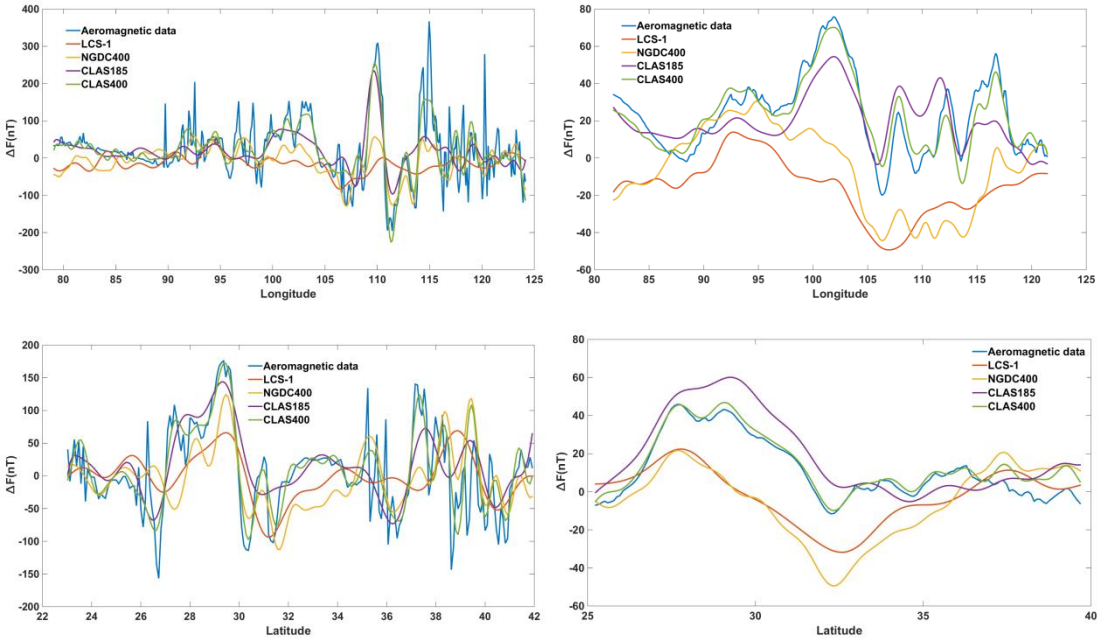

Fig 7. A comparison example of models and aeromagnetic data based on transects of grid (left) and its running averages (right).

(top: Example along longitude; bottom: Example along latitude;)

The figure shows satellite models (LCS-1: orange curve; NGDC: yellow curve) have large misfits to the data (deep blue curve), and there is no strong correlation between data and satellite models (correlation coefficients less than 0.3). In contrast, CLAS185 (purple curve) and CLAS400 (green curve) can better match the trend of the data. Especially for CLAS400, the averages match not only in trend, but also in value. These results are clearer by plotting of running averages (right of Fig. 7) which smooth some small-scale features.

Power spectrum

Lowes-Mauersberger power spectrum for satellite models and CLAS models are compared in Fig.8 and Fig.9 shows the degree correlation between two kinds of models, determined using

$$R_n = (n+1)\sum_{m=0}^{n}\left[\left(g_n^m\right)^2 + \left(h_n^m\right)^2\right] \tag{7}$$

This is a lower bound as the power spectrum is global and we only have detail locally.

For the long wavelength model, the power spectrum of CLAS133 (green line) and CLAS185 (yellow line) are in good agreement with satellite models until last few degrees. Because the degree is truncated, its power spectra rise rapidly. For degrees n<300, the power of CLAS400 and NGDC model is at the similar level. With the degree going higher, NGDC model may underestimates the global lithospheric power above degree 300, CLAS400 has more power.

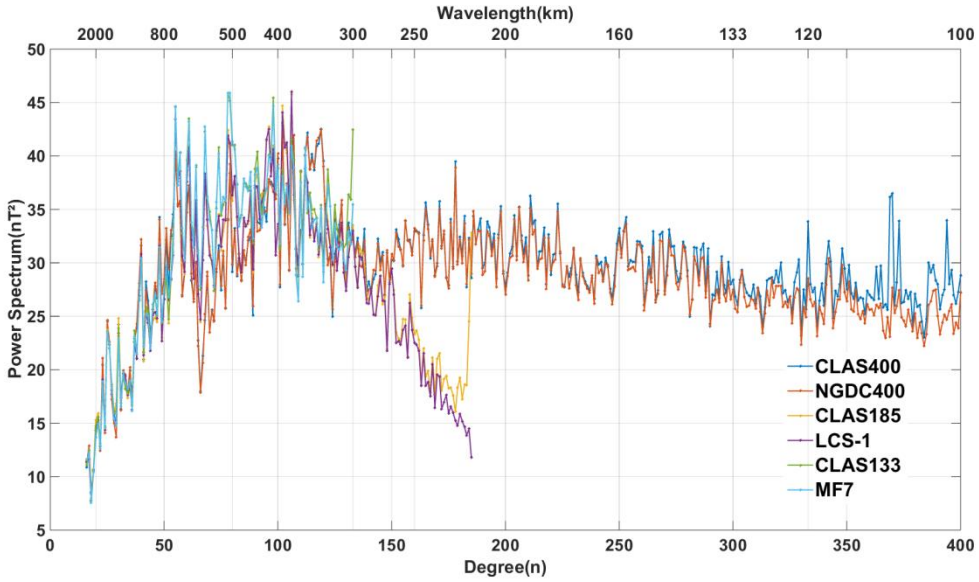

Fig 8. Lowes-Mauersberger power spectrum at Earth surface for various models

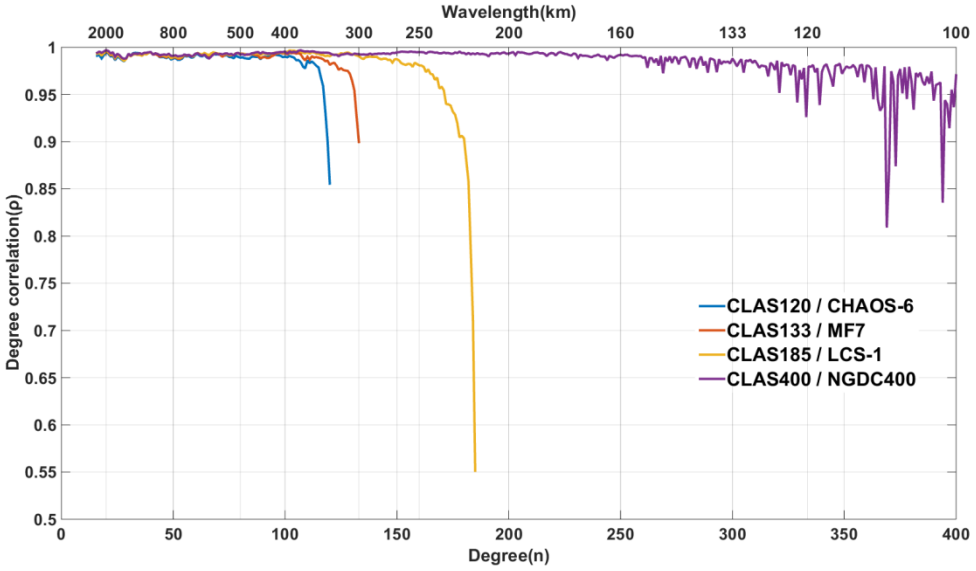

Fig 9. Degree correlation between CLAS models and satellite models

The degree correlation (Langel & Hinze, 1998) between two models $\mathbf{m}=\{g_n^m, h_n^m\}$ and $\bar{\mathbf{m}}=\{\bar{g}_n^m, \bar{h}_n^m\}$ can be calculated by

$$\rho_n = \frac{\sum_{m=0}^{n}\left(g_n^m \bar{g}_n^m + h_n^m \bar{h}_n^m\right)}{\sqrt{\left[\sum_{m=0}^{n}\left(\left(g_n^m\right)^2+\left(h_n^m\right)^2\right)\right]\left[\sum_{m=0}^{n}\left(\left(\bar{g}_n^m\right)^2+\left(\bar{h}_n^m\right)^2\right)\right]}} \tag{8}$$

Fig.9 shows CLAS models have a good agreement with satellite models at low degree. Correlation coefficients above 0.9 for CLAS120 at degree n<100, CLAS133 at degree n<120 and CLAS185 at degree n<160, respectively. But for high degree terms, degree correlation drops sharply which means that the damping makes this part constrained by aeromagnetic

data. With the weaker damping from the model, more degrees are constrained by aeromagnetic data and model will have more power. The correlation between the CLAS400 and NGDC model has always remained above 0.9, and there are some jumps after the degree 350.

Coherency

Due to the existence of small-scale structures, to better assess the long-wavelength lithosphere magnetic field of the models, aeromagnetic data are filtered with a low-pass wavelength cut off (Gubbins, 2004) of 225km and 100km by fast Fourier transform (FFT) as shown in Fig 10, with a spatial comparison of magnetic total intensity anomalies between filtered aeromagnetic data and LCS-1, NGDC and CLAS models.

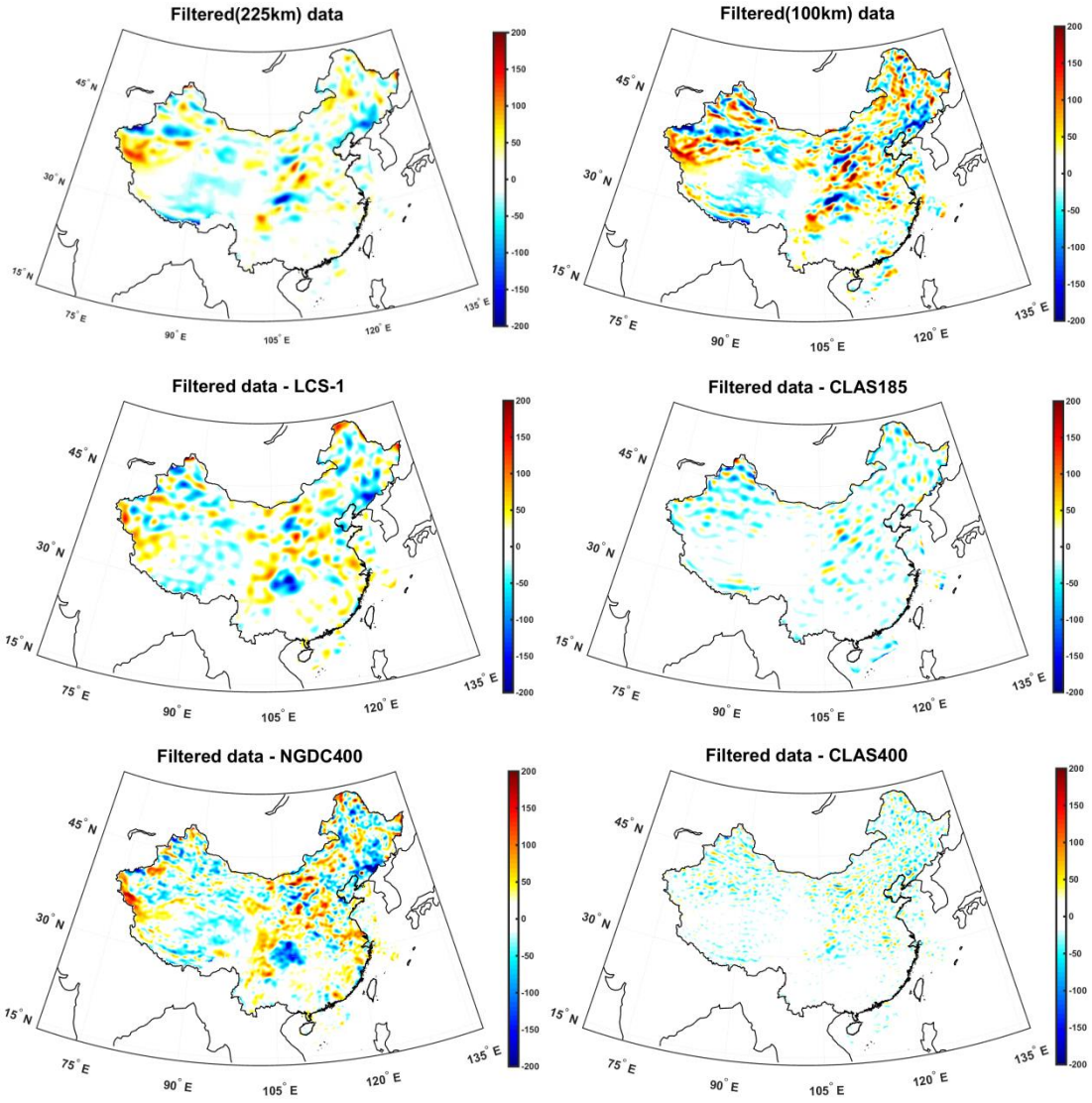

Fig 10. Comparison between filtered data and models. Units are nT.
Top: Plot of anomaly *F* low-pass filtered (left: 225km; right: 100km) aeromagnetic data.
Middle: Differences of anomaly *F* from filtered data (225km) with LCS-1 (left) and CLAS185 (right).

Bottom: Differences of anomaly *F* from filtered data (100km) with NGDC400 (left) and CLAS400 (right).

In the top panel of Fig.10, most of the magnetic anomalies in northeast and Himalayas result from small-scale structures and are filtered. The remaining magnetic anomaly features are clearly observed in the northwest, central, and northeast regions, such as the areas mentioned for CLAS models in Fig. 3, with nearly the same horizontal resolution. This result is also displayed in the middle and bottom panel of Fig.10. According to the comparison, the filtered data still have finite misfit with the satellite models, particularly noticeable in the central of China. However, there is a good correlation between filtered data and CLAS400 with correlation coefficients of 0.95. Same comparisons also made for CLAS185 with correlation coefficients of 0.9, while satellite models only have correlation coefficients of 0.53, 0.65 for LCS-1 and NGDC400, respectively.

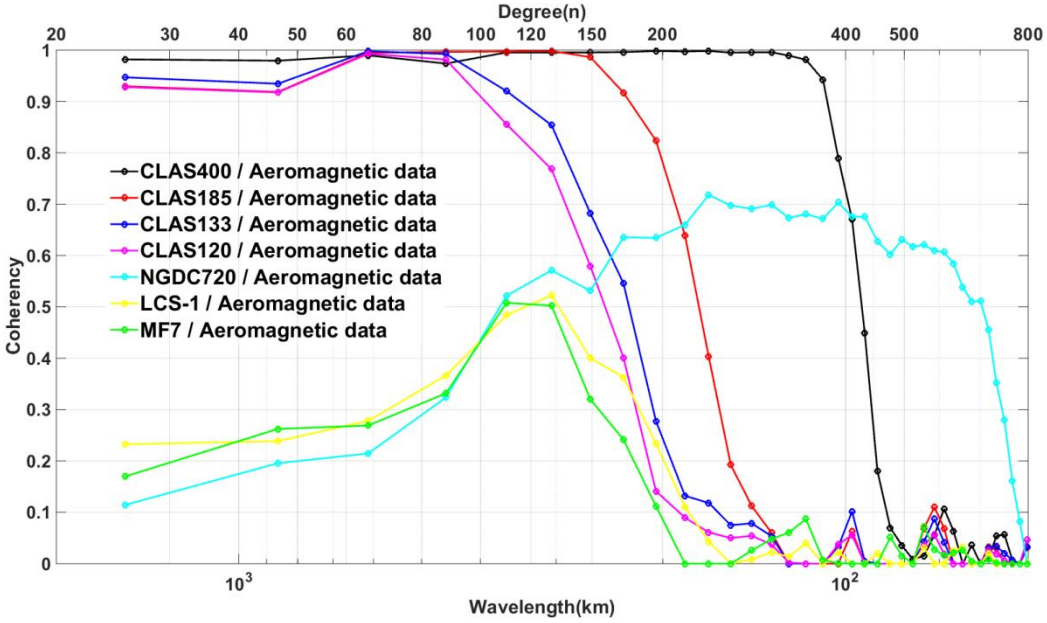

Fig 11. spectral coherence comparison between the full spectrum aeromagnetic data in the central third of China and CLAS models and satellite models.

The above comparisons also agree with the coherence estimates (Blakely, 1995) by Fourier domain calculations in the central third of China (about 23.67°*N*-41.38°*N*, 97.74°*E*-120.16°*E*) (Fig.11). Fig.11 demonstrates that satellite models differ greatly from aeromagnetic data in central China, whether it is the LCS-1 (yellow curve), MF7 (green curve) or NGDC720 (light blue curve). The coherence values of these models are broadly below 0.5 for long wavelength field, which explains the gap between the two data sets. Even for short-wavelength fields with higher degrees, the highest coherence of the NGDC model is only about 0.7. Refer to the coherence between EMM2015 (Maus et al., 2015) and Australia aeromagnetic data. The model uses the Australian aeromagnetic data for wavelengths less than 300 km (Olsen et al., 2017), thus the overall coherence is above 0.8 and the short wavelength part can reach to 0.95 or more. This result reflects the fact that the model does not

fit the Chinese aeromagnetic data and therefore can still be improved. In contrast, this gap can be filled by CLAS models. In the central China, CLAS400 (black curve) has a good coherence of 0.9 or more at the wavelengths above 108 km. Other CLAS models (CLAS185: red curve, CLAS133: deep blue curve, CLAS120: purple curve) also have similar high coherence values at long wavelengths, and degrade around wavelengths of 333, 300 and 205km. We preformed similar analysis over other regions of continental China with the same results. The coherence values of the satellite models are higher in western China (about 0.7) than in other regions, but the values in the northeast are similar to those in central region.

Conclusions

In this article, we use Chinese aeromagnetic data and global satellite models to derive regional models of Chinese lithospheric field. The models are estimated by a depleted basis of global functions and simplify calculations with symmetry and eigenvalues. This is the first time that high-quality Chinese aeromagnetic data have been combined with satellite-derived constrains for regional modeling.

Perhaps the most important result is not shown in this paper. Earlier, unsuccessful work had attempted to model directly both satellite and ground-based data, and was not successful. For global modelling, such an approach has been applied successful in, for example, the Comprehensive models (e.g., Sabaka et al., 2004; 2015), but to apply this technique to the resolution we would seek for regional modelling is not numerically feasible, not to mention problems with variations in resolution ground-based data. This motivated this current work, and we have demonstrated that by combined modelling, we may combine the best features of best-practice modelling of both satellite and ground-based data.

The results show that we are able to model the aeromagnetic data compilation with small deviations from a global model. CLAS models have substantially greater resolution than models derived from satellite data alone, and reflect more features of the lithospheric field in continental China, such as Changbai mountains, Sichuan Basin and Qinghai-Tibet Plateau. The newly derived model also better fits the large-scale trend of aeromagnetic data, CLAS400 has a good agreement (coherence>0.9) with Chinese aeromagnetic data at wavelength down to about 100km (corresponding to spherical harmonic degree n = 400), which can fill the gap between models using purely satellite or aeromagnetic data. Comparison with aeromagnetic data filtered at 100 km gives good agreement (correlation> 0.95).

The global models derived from satellite data have some clear common features with Chinese aeromagnetic data (e.g., coherence about 0.7 in western China), but there are also clear offsets (coherence<0.5) between regions, for example in central and northeast China. Newly derived models using the satellite-derived lithospheric field models as the initial model, have a high correlation with the satellite models at low degree (degree correlation>0.9), but allow much greater power at high degree.

There are substantial differences in the comparison of aeromagnetic data and CLAS models, especially in the Sichuan Basin. Using the aeromagnetic data alone, the trend of magnetic anomalies in this area is north-east. This huge strip-shaped magnetic anomaly is generally considered to arise from a very deep source. However, combining with satellite data, the magnetic anomaly direction is instead east-west, even for the long-wavelength CLAS185 model. The higher resolution CLAS400 model with smaller scale structure only strengthens this conclusion. Therefore, the addition of constraint from satellite data changes the geological interpretation fundamentally, suggesting that the source of magnetic anomaly in the Sichuan Basin is not deep.

The two data sets are not completely consistent. Damping must be added to control the balance between satellite models and aeromagnetic data, leading to an inevitable loss of model precision. Therefore, future modeling requires an improvement in the aeromagnetic line leveling. The aeromagnetic data are not actually "data", but are the output a model derived from these data - to get properly consistent data, the satellite model needs to be used as the long-wavelength filter for the processing of the lithospheric field data. Therefore, the future models should start from a reanalysis of the aeromagnetic data and its line leveling to be consistent with the satellite model. It would also be possible to model the ground data by calculating horizontal gradients by differencing data, reducing the effect of incorrect line leveling. However, our results indicate sufficiently strongly that the leveling should be corrected at source that this analysis is unlikely to be sufficient. Similarly, detailed geological analysis should await a more consistent amalgamation of the data sources.

Finally, the presented models still have large residuals (RMS above 70nT) to aeromagnetic data, arising from the small-scale structure of aeromagnetic data with wavelength less than 100km. Since that the existing models which have high spherical harmonic degrees do not use Chinese aeromagnetic data, considering shorter wavelength of aeromagnetic survey and increasing the spatial resolution of lithospheric field model in China, higher resolution models must be sought to fully integrate the satellite and ground-based data for lithospheric field modeling.

Acknowledgements

We wish to thank China Aero Geophysical Survey and Remote Sensing Center for Natural Resource for providing Chinese aeromagnetic data. Gratefully acknowledge for the support of China Scholarship Council. We would like to thank Nils Olsen, Dhananjay Ravat, Chris Finlay and Simon Williams for assistance in research. This work was funded by Macau Foundation and the pre-research project on Civil Aerospace Technologies No. D020308 and D020303 funded by China's National Space Administration, NERC grant NE/M012190/1, opening fund of State Key Laboratory of Lunar and Planetary Sciences (Macau University of Science and Technology) (Macau FDCT grant No. 119/2017/A3), China Scholarship Council (No. 201708320317), National Natural Science Foundation of China (Grant No. 41404053,

Grant No. 41604134, Grant No. 41174165, Grant No. 41974073), Special Project for Meteo-scientific Research in the Public Interest (Grant No. GYHY201306073-2), Graduate Research and Practice Innovation Program (KYCX17_0896) and the Specialized Research Fund for State Key Laboratory of Space Weather.

References

Beggan, C., Saarimaki, J., Whaler, K. A., & Simons, F. J. (2013). Spectral and spatial decomposition of lithospheric magnetic field models using spherical Slepian functions. Geophysical Journal International, 193(1), 136-148.

Blakely, R. (1995). Potential Theory in Gravity and Magnetic Applications. Cambridge University Press.

De Santis, A., Torta, J. M., & Falcone, C. (1996). A simple approach to the transformation of spherical harmonic models under coordinate system rotation. Geophysical Journal International, 126(1), 263-270.

Finlay, C. C., Olsen, N., & Toffnerclausen, L. (2015). DTU candidate field models for IGRF-12 and the CHAOS-5 geomagnetic field model. Earth, Planets and Space, 67, 114.

Finlay, C. C., Olsen, N., Kotsiaros, S., Gillet, N., & Tøffner-Clausen, L. (2016). Recent geomagnetic secular variation from Swarm. Earth, Planets and Space, 68(1), 1-18.

Feng, Y., Jiang, Y., Jiang, Y., Li, Z., Jiang, J., & Liu, Z. W., et al. (2016a). Regional magnetic anomaly fields: 3d taylor polynomial and surface spline models. Applied Geophysics, 13(1), 59-68.

Feng, Y., Jiang, Y., Jiang, Y., Liu, B. J., Jiang, J., & Liu, Z, W. (2016b). Spherical cap harmonic analysis of regional magnetic anomalies based on champ satellite data. Applied Geophysics, 13(3), 561-569.

Feng, Y., Holme, R., Cox, G. A., & Jiang, Y. (2018). The geomagnetic jerk of 2003.5-characterisation with regional observatory secular variation data. Physics of the Earth and Planetary Interiors, 47-58.

Friischristensen, E., Luhr, H., & Hulot, G. (2006). Swarm : A constellation to study the Earth's magnetic field. Earth, Planets and Space, 58(4), 351-358.

Gubbins, D. (2004). Time Series Analysis and Inverse Theory for Geophysicists, Cambridge Univ. Press.

Haines, G. V. (1985). Spherical cap harmonic analysis. Journal of Geophysical Research: Solid Earth, 90(B3), 2583-2591.

Hemant, K., Thébault, E., Mandea, M., Ravat, D., & Maus, S. (2007). Magnetic anomaly map of the world: merging satellite, airborne, marine and ground-based magnetic data sets. Earth and Planetary Science Letters, 260(1), 56-71.

Langel, R.A. & Hinze,W.J., 1998. The Magnetic Field of the Earth's Lithosphere: The Satellite Perspective, Cambridge Univ. Press.

Lesur, V., Hamoudi, M., , Choi, Y., Dyment, J. & Thébault, E. (2016) Building the

second version of the World Digital Magnetic Anomaly Map (WDMAM), *Earth, Planets and Space* **68**:27 DOI 10.1186/s40623-016-0404-6

Maus, S., Luhr, H., Rother, M., Hemant, K., Balasis, G., Ritter, P., & Stolle, C. (2007). Fifth-generation lithospheric magnetic field model from CHAMP satellite measurements. Geochemistry Geophysics Geosystems, 8(5).

Maus, S., Yin, F., Lühr, H., Manoj, C., Rother, M., Rauberg, J., ... & Müller, R. D. (2008). Resolution of direction of oceanic magnetic lineations by the sixth - generation lithospheric magnetic field model from CHAMP satellite magnetic measurements. Geochemistry, Geophysics, Geosystems, 9(7).

Maus, S. (2010a). Magnetic field model MF7. Available at: https://www.geomag.us/models/MF7.html, last accessed 1 September 2017.

Maus, S. (2010b). An ellipsoidal harmonic representation of Earth's lithospheric magnetic field to degree and order 720. Geochemistry, Geophysics, Geosystems, 11(6).

Maus, S., (2015). Enhanced Magnetic Model (EMM2015). Available at: https://www.ngdc.noaa.gov/geomag/EMM/.

Milligan, P., Franklin, R., Minty, B., Richardson, L. & Percival, P., (2010). Magnetic anomaly map of australia (5th edn), 1:5 000 000 scale (digital data set at geophysical archive data delivery system), Tech. Rep., Geoscience Australia, Canberra.

Olsen, N., Lühr, H., Finlay, C. C., Sabaka, T. J., Michaelis, I., Rauberg, J., & Tøffner-Clausen, L. (2014). The CHAOS-4 geomagnetic field model. Geophysical Journal International, 197(2), 815-827.

Olsen, N., Ravat, D., Finlay, C. C., & Kother, L. K. (2017). LCS-1: a high-resolution global model of the lithospheric magnetic field derived from CHAMP and Swarm satellite observations. Geophysical Journal International, 211(3), 1461-1477.

Ou, J. M., Du, A. M., E. Thébault, Xu, W. Y., & XiaoBo Tian, et al. (2013). A high resolution lithospheric magnetic field model over china. Science China, 56(10), 1759-1768.

Ravat, D., & Korhonen, J. (2009). A preliminary, full spectrum, magnetic anomaly grid of the united states with improved long wavelengths for studying continental dynamics. Center for Integrated Data Analytics Wisconsin Science Center, 12(1), 349-364.

Sabaka, T. J., Olsen, N., & Purucker, M. E. (2004). Extending comprehensive models of the Earth's magnetic field with Ørsted and CHAMP data. Geophysical Journal International, 159(2), 521-547.

Sabaka, T. J., Olsen, N., Tyler, R. H., & Kuvshinov, A. (2015). CM5, a pre-Swarm comprehensive geomagnetic field model derived from over 12 yr of CHAMP, Ørsted, SAC-C and observatory data. Geophysical Journal International, 200(3), 1596-1626.

Simons, F. J., Dahlen, F. A., & Wieczorek, M. A. (2006). Spatiospectral concentration on a sphere. SIAM review, 48(3), 504-536.

Thébault, E., Schott, J. J., & Mandea, M. (2006). Revised spherical cap harmonic analysis (R-SCHA): Validation and properties. Journal of Geophysical Research: Solid

Earth, 111(B1).

Thébault, E., Purucker, M., Whaler, K. A., Langlais, B., & Sabaka, T. J. (2010). The magnetic field of the Earth's lithosphere. Space Science Reviews, 155(1-4), 95-127.

Xiong, S. Q., Tong, J., Ding, Y. Y., & Li, Z. K. (2016a). Aeromagnetic data and geological structure of continental China: A review. Applied Geophysics, 13(2), 227-237.

Xiong, S. Q., Yang, H., Ding, Y., Li, Z., & Li, W. (2016b). Distribution of igneous rocks in China revealed by aeromagnetic data. Journal of Asian Earth Sciences, 129, 231-242.